ELSEVIER

Journal of Biomechanics 41 (2008) 1953–1960

JOURNAL OF BIOMECHANICS

www.elsevier.com/locate/jbiomech
www.JBiomech.com

Stepwise reduction of functional spinal structures increase disc bulge and surface strains

Frank Heuer, Hendrik Schmidt, Hans-Joachim Wilke*

Institute of Orthopaedic Research and Biomechanics, University of Ulm, Helmholtzstr. 14, 89081 Ulm, Germany

Accepted 28 March 2008

Abstract

Previous studies postulated that an axial compression of lumbar intervertebral discs causes a complex strain pattern on the annulus. This pattern is not fully understood, since most studies measured only the uniaxial ultimate tensile strain of the annulus. The aim of this study was to investigate surface strains and their relation to disc bulging. This work was extended to study some defects that are relevant for the intermediate process of finite element modeling.

Six specimens (L2–3) with a median age of 51 years were utilized for this in vitro study. Specimens were loaded with pure moments (2.5–7.5 N m) in the principal directions. The anatomy was subsequently reduced in three steps: (1) ligamentous and bony posterior structures, (2) anterior and posterior ligaments and (3) nucleus. Measured were ranges of motion, three-dimensional disc bulging and surface strains of the outer annulus.

Lateral bending showed the largest axial strains (9.7%) for intact specimens, which increased to 15.1% after the removal of posterior structures. Disc bulging was largest in flexion with 1.56 mm, which increased to 2.06 mm after step (1). Defect (2) caused that flexion yielded the largest axial strains with 22.6% and 2.17 mm of bulging. We could also determine a constriction effect of these ligaments. Nucleotomy did not essentially increase anterior disc bulging in flexion, but inward disc bulging increased by 0.55 mm, in extension.

Due to the increase in the complexity of finite element models, it is difficult to obtain data from the literature for validation purposes. This study presents new data, which assist in the development of such models.

Keywords: Disc bulging; Disc contour; Lumbar spine; Soft tissue; Surface strains; Calibration; Validation; Finite element model

1. Introduction

In previous studies, it was stated that already an axial compression of lumbar spinal segments causes a complex strain pattern to the outer annulus surface (Bruehlmann et al., 2004a; Shah et al., 1978). This pattern is not fully understood, since most studies investigated only uniaxial ultimate tensile properties of the annulus. These tensile tests yielded strains in axial, circumferential or in fiber direction. These tests were usually performed until structural failure occurred. It was reported that the annulus can resist axial strains (strain in caudal–cranial direction) of 20% (Wagner and Lotz, 2004) to 50% (Green et al., 1993) and circumferential strains of 10% (Ebara et al., 1996; Green et al., 1993) to 21% (Iatridis et al., 2005). Testing of undamaged intervertebral discs (IVD) resulted in maximal circumferential strains with more than 50% in a study by Shah et al. (1978). However, some fiber strain measurements of intact discs were presented in a few works (Klein et al., 1983; Stokes, 1988). From this point, it might be suggested to study the interaction of the axial, circumferential strains by assessing all strain components on an undamaged IVD with the working functional annulus. Still, less is known about the surface strain distribution of IVD for non-destructive loading.

Uniaxial loading and the stress and strain characteristics of IVDs were investigated by other groups using numerical models (Goel et al., 1995; Meakin et al., 2001; Rohlmann et al., 2006; Shirazi-Adl et al., 1984). These finite element (FE) models were validated using merely one- or

*Corresponding author. Tel.: +49 731 500 55301; fax: +49 731 500 55302.
E-mail address: hans-joachim.wilke@uni-ulm.de (H.-J. Wilke).

0021-9290/$ - see front matter © 2008 Elsevier Ltd. All rights reserved.
doi:10.1016/j.jbiomech.2008.03.023

two-dimensional displacement or disc bulging data from in vitro experiments (Brinckmann, 1986; Brown et al., 1957; Stokes, 1988; Wenger and Schlegel, 1997). Strain data for physiological loading of the disc would be more sufficient in the validation, since the intervertebral disc is the component in the spine, which deforms most under load.

In two previous in vitro studies, we provided various data regarding rotational (Heuer et al., 2007b), translational range of motion (RoM), intradiscal pressure (Heuer et al., 2007a) and three-dimensional disc displacement (Heuer et al., 2008a). These experiments were especially designed to assist in the processes of FE model development, calibration (Schmidt et al., 2007a; Schmidt et al., 2006) and the subsequent validation (Noailly et al., 2007; Rohlmann et al., 2007; Schmidt et al., 2008; Schmidt et al., 2007b). The purpose of this study was to provide new data of the three-dimensional disc bulging and surface strains of the outer annulus fibrosus in a similar experimental sequence, as it was presented before (Heuer et al., 2007a, b).

2. Methods

2.1. Specimen preparation

This investigation was performed with the same set of human donor spines (Heuer et al., 2007b). The former study utilized L4–5 segments, but this current study used the segment level above (L2–3). Six of these lumbar spinal segments were included in this study, having a median age of 51 years (ranging from 38 to 59). The soft tissue was carefully removed, not harming the ligaments, facet capsules and the IVD. Before potting, specimens were rigged using a fixture, ensuring an optimal IVD alignment. Specimens were orientated so that the mid-horizontal IVD plane was in parallel to the lower casting mold. Then, the cranial and the caudal end of the segments were potted.

Six pins with a diameter of 1.0 mm were implanted near the endplates, three pins above and three pins below the IVD (Fig. 1(a)). Pins were placed to stick out by 3 mm. This was performed to ensure a segmentation of the IVD in the scanning data. The vertebral bodies and the IVD were coated with an artificial roughness pattern to the surface (Fig. 1(b)). This produced a randomized and stochastically distributed "salt-and-pepper" pattern to the disc surface, which was required to detect surface deformation using image-processing algorithms (Sutton et al., 2000).

2.2. Experimental protocol

A laser scanner was mounted on the spine tester frame before starting the experiments. This sensor can spatially digitize the surface of the lumbar segments, while a bending or compression load is applied to specimens in the spine tester (Heuer et al., 2008b). This laser scanner provides an accuracy of 10 μm in radius, 25 μm in height and 0.04° in the circumference. However, the caudal ends of L3 were affixed to the laser scanner base. The cranial ends of L2 were connected to the spine tester gimbal (Wilke et al., 1994). Initially, a defined preload of 500 N was applied to specimens for 15 min for preconditioning. Subsequently, a baseline scan of the three-dimensional IVD contour was acquired from the unloaded specimens. Surface data consisted of 512 points in cranial–caudal direction and 720 points along the circumference (Fig. 1(c)). After the initial scan, 500-N axial compression or pure unconstraint bending moments were applied. Moments were varied between 2.5, 5 and 7.5 N m. Specimens were exposed to flexion, extension, lateral bending and axial rotation movements. Maximal deflections were evaluated from the RoM assessment. For the surface data acquisition, specimens were brought into the maximal deflections and held. This was followed by an immediate surface scan in this position. A scan took 4 s and it can be assumed that the viscoelastic behavior of the IVDs under a constant load did not significantly change the IVD contour (Heuer et al., 2007c). IVD contour scans were recorded for all directions driven.

After the intact measurements were accomplished, three further defects were studied in accordance with the protocol. In the first defect, the posterior structures such as the vertebral arches and facet joints were removed, including the removal of the supraspinous, interspinous and flaval ligaments (w/oVA). In the next step, the posterior (PLL) and the anterior longitudinal ligaments (ALL) were removed, which were assigned to be the w/oALL defect. In the last reduction step, the nucleus pulposus was removed (mean nucleus mass 2.9 g) in order to study pure annulus behavior (w/oNUC). For the NUC defect, a small oblique incision into the IVD was performed from a right posterplateral approach (6–7 mm wide). This access was oriented along a fiber direction, preserving the annulus fibers in this direction. The nucleus pulposus was extracted using rongeurs. These defects and the abbreviations were defined in accordance with the first similar biomechanical investigation (Heuer et al., 2007b).

2.3. Data evaluation

The second loading cycle of the spine tester was used to determine the RoM. RoM data were statistically evaluated using the Wilcoxon signed rank test within the group. Since the test has an explorative character, a correction for multiple testing has been omitted.

Surface scan data were assigned to a grayscale-alike pattern, which allowed for a determination of displacement vectors between surface data obtained from specimens in a loaded and unloaded situation (Heuer et al., 2008b). In principle, these displacement maps were determined by correlating image data from the scanned surface data sets, comparing the undeformed with the deformed situation. Surface strains were computed from these displacement maps using the FE analysis software package Ansys V11.0 (Swanson Analysis, Houston, PA, USA). Nodes (IVD surface points) together with the element table were transferred to ANSYS. Displacements of each node were provided as boundary conditions for the solver. The surface strains in the circumference ($\varepsilon_{\phi-\phi}$) and axial direction (ε_{z-z}) were computed for each element. Disc bulging was determined in a similar way. The displacement vectors also contained the information of the upper vertebra translation. This translation has been subtracted from the deformation map using the FE analysis software. This then yielded relative disc bulging. That means the relative disc

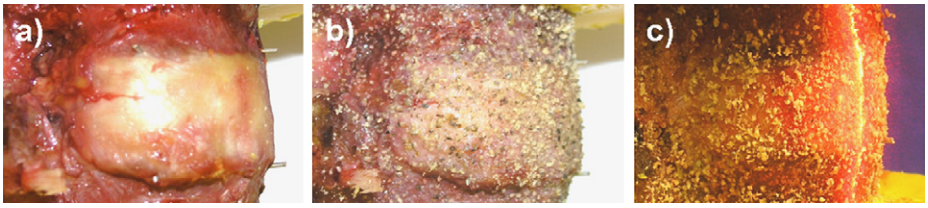

Fig. 1. (color online) (a) Side view of L2–3 specimens with six steel pins for segmenting both endplates; (b) surface roughness was coated on the specimen surface, which was required for the image registration procedures; (c) shows a profile line, which was projected and acquired by the laser scanner device inside the spine testing machine. Spatial data of the surfaces were obtained by rotating the sensor about the specimen.

bulging contained the out-of-plane deformation without the initial disc contour and without translation of the upper vertebra. It was distinguished between outward and inward disc bulging of the outer annulus surface. All data were summarized using the median function. Disc bulging values were also summarized for four anatomical landmarks: the middle anterior, the middle left lateral, the middle left posterolateral and the middle posterior point (Heuer et al., 2008a).

3. Results

For 7.5 N m, intact specimens yielded RoMs of 5.2°, 3.4°, 5.8° and 2.2° in flexion, extension, lateral bending and axial rotation, respectively (Table 1). For flexion, surface strains resulted in maximum values of 3.7% in circumferential and 7.2% in axial direction (Table 2 and Fig. 2). In flexion, a maximal outward disc bulging of 1.56 mm was obtained at the frontal region (Table 3, Figs. 3 and 4). Extension showed a maximum circumferential strain of 1.5%, maximal 3.4% strain in the axial direction and an anterior inward bulging with −0.67 mm. Largest axial strains were found for lateral bending having 9.7%. Lateral bending showed an outward bulging of 1.20 mm and an inward bulging of −0.82 mm at the contralateral side of bending. Axial compression resulted in 2% for $\varepsilon_{\phi-\phi}$ and 2.6% for ε_{z-z}. The strain distribution showed negative axial strain values near the endplates, indicating compression zones (Fig. 2).

The w/oVA defect increased the RoM in all directions. In flexion, the neural arch removal enlarged the motion by 1.1°, whereas in extension the RoM increased by 2.5°. Lateral bending showed a slight increase by 0.7° due to the defect. In axial rotation, the RoM doubled compared to the intact condition. Except for axial compression, the maxima of the circumferential strains strongly increased in all directions. Flexion yielded 13.6% axial and 10% circumferential strain, also resulting in 2.06 mm outward disc bulging. Extension yielded 1.05 mm inward disc bulging and 1.17 mm outward bulging at the anterior and posterior point, respectively (Table 3). Again, lateral bending resulted in the largest axial strain with 15.1% and 1.41 mm outward bulging.

Table 1
Median values of the range of motion in degrees of six L2–3 segments as a function of the bending moment and reduction stages

Loading direction	Bending moment in N m	Anatomical reduction stage of L2–3 segments			
		INTACT	w/oVA	w/oALL	w/oNUC
Flexion	2.5	2.09	3.04	3.74	7.84
	5	4.25	4.89	5.44	10.25
	7.5	5.20	6.31	6.92	11.55
Extension	2.5	1.34	2.94	4.03	8.13
	5	2.63	4.80	6.21	9.85
	7.5	3.36	5.88	8.20	11.50
Right lateral bending	2.5	2.94	3.64	3.80	5.41
	5	4.57	5.13	5.39	6.96
	7.5	5.79	6.44	6.64	8.34
Left axial rotation	2.5	0.70	1.63	1.76	3.98
	5	1.74	2.84	3.06	5.54
	7.5	2.15	3.93	4.06	6.80

Table 2
Maximum values of the median surface strains ($n = 6$) expressed in the axial (z–z), circumferential (ϕ–ϕ) direction

Stage	Load direction	$\varepsilon_{\phi-\phi}$ (%)		ε_{z-z} (%)	
		Max.	Min.	Max.	Min.
INTACT	Axial compression	2.0	−2.1	2.6	−4.7
	Flexion	3.7	−7.6	7.2	−12.7
	Extension	1.5	−3.0	3.4	−4.9
	Lateral bending	4.1	−7.1	9.7	−17.3
	Axial rotation	0.8	−2.7	1.8	−2.1
w/o VA	Axial compression	2.7	−3.7	3.0	−8.8
	Flexion	10.0	−8.4	13.6	−13.4
	Extension	4.2	−5.8	6.1	−13.2
	Lateral bending	9.4	−7.0	15.1	−19.7
	Axial rotation	2.2	−3.5	2.7	−4.7
w/o ALL	Axial compression	3.5	−3.4	3.0	−10.4
	Flexion	13.8	−7.0	22.6	−15.0
	Extension	9.0	−11.3	12.8	−28.0
	Lateral bending	10.9	−9.4	17.3	−18.0
	Axial rotation	2.0	−6.4	4.3	−6.4

Specimens were exposed to bending moments of 7.5 N m or an axial compressive load of 500 N. Three defect stages and the INTACT condition were considered.

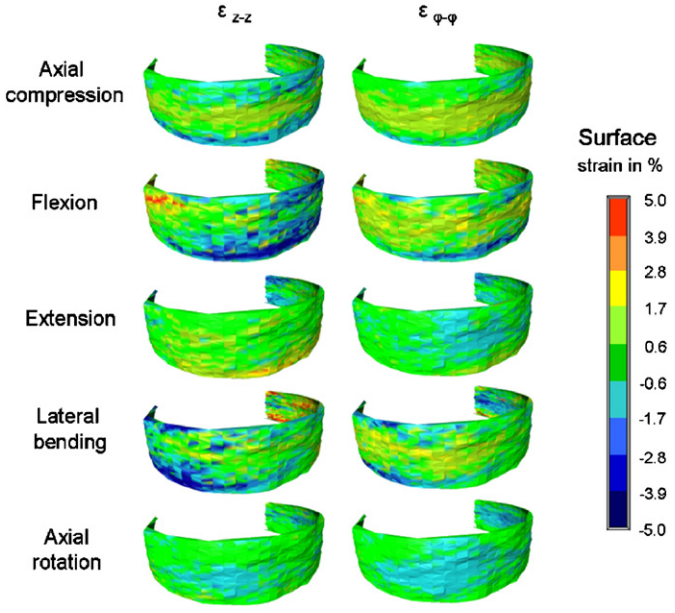

Fig. 2. Surface strains in axial direction (ε_{z-z}) and circumferential direction ($\varepsilon_{\varphi-\varphi}$) of intact specimens from a right frontal view. Specimens were loaded with bending moments of 7.5 N m in flexion, extension, right lateral bending and left axial rotation. Furthermore, an axial compression of 500 N was evaluated. The posterior region of the discs has a gap, because this region could not be accessed in the intact specimens with the scanner.

Table 3
Median, minimum and maximum values in millimeters of disc bulging data evaluated for the four landmarks

Loading direction	Specimen state	Landmarks											
		Anterior			Lateral			Posterolateral			Posterior		
		Median	Min.	Max.	Median	Min.	Max.	Median	Min.	Max.	Median	Min.	Max.
Axial load 500 N	INTACT	0.70	0.57	0.79	0.23	−0.02	0.52	–			–		
	w/oVA	0.79	0.21	1.77	0.51	0.13	0.95	0.30	−0.29	0.42	0.15	−0.10	0.58
	w/oALL	0.64	0.04	1.05	0.83	0.44	0.98	0.38	−0.07	0.60	0.33	0.09	0.56
	w/oNUC	−0.03	−0.83	1.86	0.30	−0.68	0.83	0.33	−0.25	0.42	0.28	−0.08	0.62
Flexion	INTACT	1.56	0.94	1.96	0.10	−0.23	0.21	–			–		
	w/oVA	2.06	1.28	2.54	0.21	−0.33	0.41	−0.77	−0.97	−0.52	−0.83	−1.04	−0.72
	w/oALL	2.17	1.34	2.70	0.12	−0.57	0.37	−0.92	−1.08	−0.45	−0.91	−1.26	−0.57
	w/oNUC	2.09	1.47	3.37	−0.13	−0.94	0.16	−1.27	−1.62	−0.52	−1.27	−1.56	−0.74
Extension	INTACT	−0.67	−1.17	−0.43	0.33	−0.22	0.43	–			–		
	w/oVA	−1.05	−1.36	−0.51	0.49	0.05	0.77	1.10	0.66	1.17	1.17	0.63	1.43
	w/oALL	−1.36	−1.68	−0.74	0.48	−0.28	0.95	1.36	0.88	1.76	1.35	0.63	2.02
	w/oNUC	−1.91	−2.48	−1.29	0.23	−1.02	0.66	1.44	0.63	1.69	1.33	0.58	2.07
Right lateral bending	INTACT	0.26	−0.02	0.59	−0.82	−1.21	−0.47	–			–		
	w/oVA	0.45	−0.13	0.58	−1.10	−1.29	−0.87	−0.35	−0.67	−0.19	0.03	−0.19	0.26
	w/oALL	0.37	−0.06	0.60	−1.19	−1.24	−0.87	−0.35	−0.59	−0.19	0.10	−0.07	0.21
	w/oNUC	−0.51	−1.21	0.44	−1.81	−1.99	−1.47	−0.96	−1.03	−0.28	−0.13	−0.31	0.42
Left lateral bending	INTACT	0.06	−0.12	0.19	1.20	0.72	1.82	–			–		
	w/oVA	0.32	−0.04	0.49	1.41	0.97	1.73	0.47	0.02	0.86	0.08	−0.11	0.16
	w/oALL	0.35	−0.20	0.50	1.53	1.24	1.86	0.54	0.02	0.70	0.10	−0.29	0.36
	w/oNUC	−0.54	−1.17	−0.08	1.55	1.45	1.94	0.19	0.00	0.88	−0.29	−0.67	0.06
Left axial rotation	INTACT	−0.42	−0.77	−0.13	0.04	−0.24	0.34	–			–		
	w/oVA	−0.16	−0.30	0.03	−0.47	−0.83	−0.34	−0.13	−0.68	0.36	−0.16	−0.37	0.16
	w/oALL	−0.17	−0.46	−0.05	−0.53	−1.08	−0.30	−0.17	−0.42	0.21	−0.15	−0.43	0.41
	w/oNUC	−0.59	−1.46	−0.11	−0.62	−1.00	−0.19	−0.30	−0.78	0.68	−0.33	−0.87	0.31
Right axial rotation	INTACT	−0.51	−0.64	−0.19	−0.11	−0.22	0.03	–			–		
	w/oVA	−0.26	−0.54	−0.12	−0.30	−0.44	0.20	−0.34	−0.63	0.08	−0.20	−0.37	0.09
	w/oALL	−0.38	−0.58	−0.06	−0.31	−0.51	0.22	−0.35	−0.61	−0.14	−0.09	−0.38	0.10
	w/oNUC	−1.08	−1.74	−0.55	−0.31	−0.87	−0.01	−0.74	−0.96	−0.46	−0.17	−0.55	0.02

These landmarks were located at the middle disc height at the anterior, left lateral, left posterolateral and posterior region. Positive numbers indicate outward disc bulging and negatives inward bulging.

Removal of the PLL and ALL resulted in a larger increase in extension with 2.3° for 7.5 N m. This motion increased less in flexion with 0.6° for 7.5 N m. Disc bulging was affected only in a minor range. The w/oALL defect yielded the maximal axial strain in flexion with 22.6% and 13.8% in the circumferential direction. The w/oALL defect also influenced the circumferential strain distribution (Fig. 5). In extension, the w/oALL defect produced a negative strain in $\phi-\phi$ direction at the PLL location. With the PLL in place the strain showed a positive sense. In flexion, however, this removal was more pronounced in the z–z direction. Here, the strain at the PLL location changed to the negative values after the removal of the PLL.

Nucleotomy exhibited the most unstable situation. The RoM increased to 11.6°, 11.5°, 8.3° and 6.8° for flexion, extension, lateral bending and axial rotation, respectively. Outward disc bulging did not essentially increase compared to the w/oALL defect, although the inward bulging of the outer annulus increased strongly due to w/oNUC defect. For example, in extension the inward bulging increased from 1.36 mm (w/oALL) to 1.91 mm (w/oNUC).

4. Discussion

The purpose of this study was to determine IVD deformation characteristics by means of surface strains and disc bulging. This was studied on intact specimens and on three defects. These defects included the removal of bony posterior structures, all major ligaments and, in the last step, the nucleus. Data yielded surface strains and three-dimensional disc bulging, which support the development of FE models.

In the past, it was assumed (Bruehlmann et al., 2004a; Shah et al., 1978) that spinal segments under load create a complex strain pattern at the IVD surface and these were also measured (Bruehlmann et al., 2004b) . Our results showed that most load situations have a relationship between axial and circumferential strains. Maximal axial

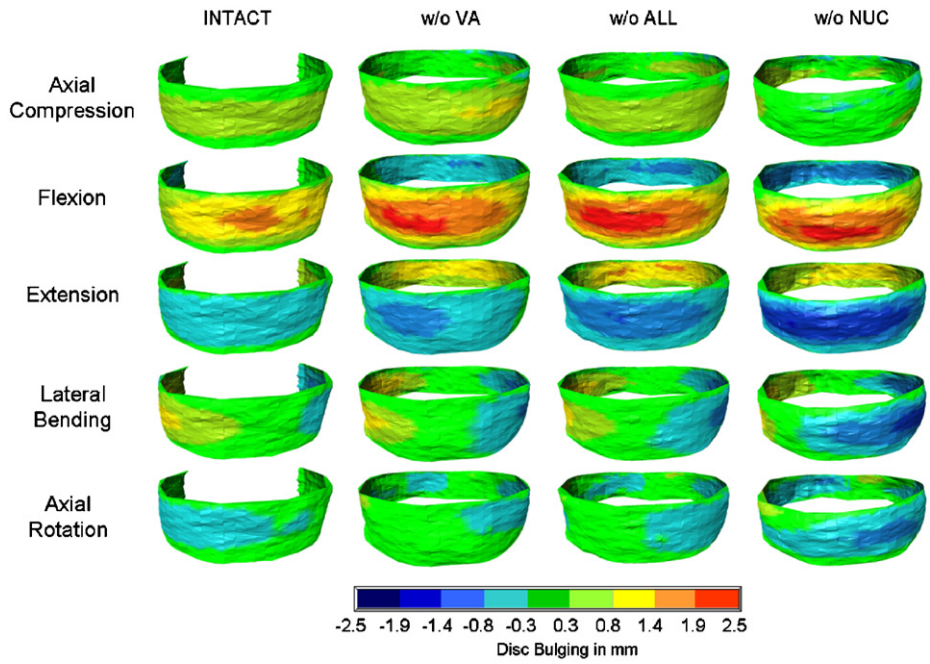

Fig. 3. Disc bulging as a function of spinal structure resection starting with intact discs (INTACT), spinal segments without the vertebral arches (w/oVA), segments without the anterior and posterior longitudinal ligaments (w/oALL) and after the removal of the nucleus (w/oNUC). The maps are depicted in a frontal view. The posterior region of the intact discs has a gap, because this region could not be accessed in the intact specimens with the scanner.

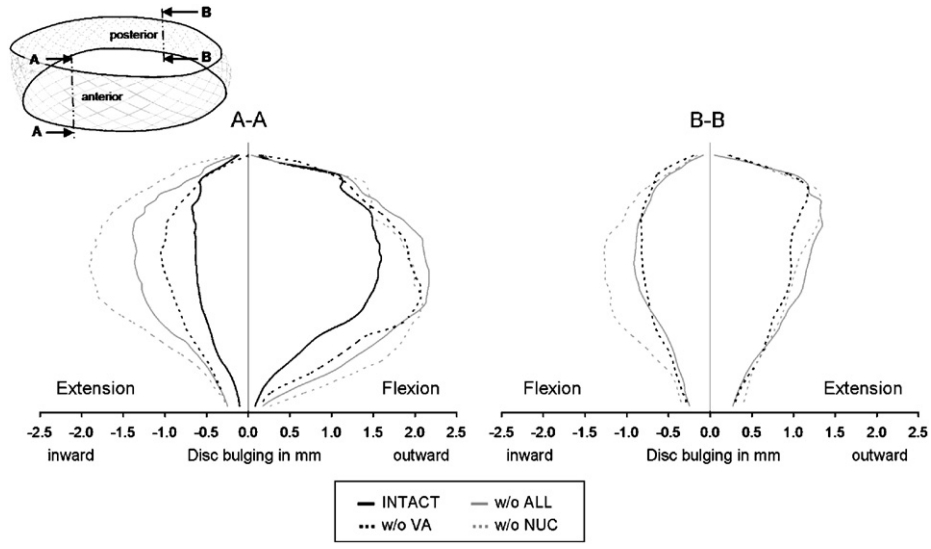

Fig. 4. In flexion and extension, relative disc bulging was evaluated for the four tested conditions: intact (INTACT), without vertebral arches (w/oVA), without the longitudinal ligaments (w/oALL) and without the nucleus (w/oNUC). Presented are sagittal cuts through surface data at the frontal and posterior region. Disc heights were normalized in all specimens.

strains were almost twice the circumferential strains in flexion, extension and lateral bending for most load cases. In axial rotation, axial strains were only slightly greater than circumferential strains.

It was demonstrated that largest negative strain regions were close to the endplates. This might be because a very stiff material (vertebral bodies) interconnects to a much softer material. The point with the highest difference of stiffness is the interconnection zone also causing largest strain. It can be speculated that this region is likely the region where disc failure starts first. This assumption can be fostered by Green et al. (1993), who also showed that failure of the bone–annulus–bone specimens mostly occurred near the endplates. Previous tensile tests demonstrated that the hyaline cartilage endplate interface stripped off by pulling out the fibers from the matrix (Green et al., 1993). In experiments, we found that the axial strain was negative near both anterior endplates in flexion. Disc

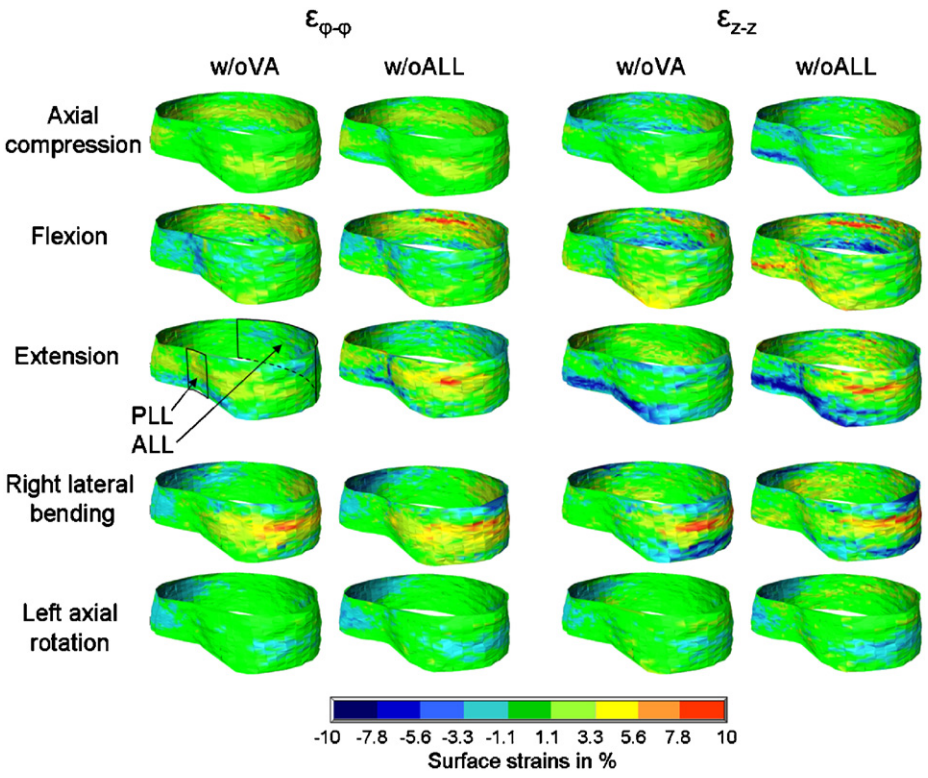

Fig. 5. Influence of the anterior (ALL) and posterior longitudinal ligament (PLL) removal (w/oALL) expressed by means of surface strains in the circumferential ($\varepsilon_{\varphi-\varphi}$) and axial direction ($\varepsilon_{z-z}$). Data are represented by median values, summarizing the six specimens. Surface strains are shown in a posterolateral view.

bulging stretched the disc in the middle causing a positive axial strain in the middle disc height. This bulging also caused a positive circumferential strain in the region of bulging. It seems that these surface strains and the disc bulging might be related to each other. However, this might not account for axial rotation.

The nucleotomy was not evaluated for the surface strains, because measurements showed that the surface strains tend to decrease after the nucleus removal. We hypothesize that these data could be due to the large deformations causing strains underestimation. Therefore, these data should be interpreted with care. This, however, needs to be confirmed by a future experiment.

The literature only described studies dealing with the testing of sectioned annulus samples (Frei et al., 2001; Hutton et al., 1999; Lotz et al., 1998). Wagner and Lotz (2004) found about 25% of strain in axial tension. Green et al. (1993) reported axial failure strain with more than 50% for the outer anterior and more than 30% strain for the outer posterior annulus. Our findings showed generally lower strains for the non-destructive loading produced with 7.5 N m. Acaroglu et al. (1995) showed that degeneration of the annulus has an influence on the failure strain and is region dependent. It was also shown that the outer anterior and posterior regions need a higher failure stress (but lower failure strain) compared to the inner layers of the annulus. Our results showed that the posterior strains were higher than anterior strains, confirming that the posterior region is more flexible than the anterior region. Furthermore, it was seen that the posterior and the ALL shielded the strain from the IVDs. Former findings already showed that the PLL and ALL had an influence on the RoM response (Heuer et al., 2007b). This study can now show that the ligaments stabilize the disc and prevent the disc from bulging. However, it cannot clearly be stated that this increase in disc bulging has arisen from the constriction effect or the increase of the RoM. A displacement-controlled load protocol would have been better to distinguish this effect.

Various values of failure strains in circumferential direction were measured, resulting in 10% in a study by Wagner and Lotz (2004). Ebara et al. (1996) reported similar strain values of about 10%. Iatridis et al. (2005) tested extracted annulus samples in a circumferential direction. It was found that the annulus samples were stretched up to 21% before rupturing. Our measurements were performed in a non-destructive loading mode, showing that intact specimens yielded a maximum of 4.1% strain in the circumferential direction for lateral bending. Removal of the posterior structures increased this value up to 13.8% for flexion being without a damage of the discs.

In general, it seems that the ultimate tensile strain upon annulus failure is higher when the annulus was stretched in an intact disc compared to the tensile testing of isolated annulus samples. Our study showed maximum axial strains

of 22.6% for the w/oVA defect. Shah et al. (1978) measured circumferential strains up to 50% at the anterior site and up to 70% posterior and 80% at the posterolateral outer annulus of intact IVDs. The testing was performed in axial compression. They also measured radial disc bulging as a function of 1500 N axial compression. Bulging was posterior with 0.9 mm larger than anterior with approximately 0.7 mm. These bulging values were comparable to our results. It was postulated that lower strains of 10% (Ebara et al., 1996) in circumferential direction can cause annulus failure of the cut samples. These lower strains are in contrast to studies measuring on intact discs. This could mean that due to the structure tensioning a too high lateral contraction occurs. We assume that this could be due to the biaxial loading characteristics of the disc. A lateral contraction can then lead to a threatened acceleration of structural failure of the sectioned samples.

A comparison of the disc bulging to former studies can only be done for the axial compression load case, because the majority of previous disc bulging studies were limited to this load application. Furthermore, most studies have created the w/oVA defect to be able to access the posterior and posterolateral disc region for measurements. Generally, our findings were in good agreement to studies reported earlier (Brinckmann, 1986; Brown et al., 1957; Hirsch and Nachemson, 1954). For example, Brinckmann (1986) reported a posterolateral bulging of 0.2 mm for 1000 N of compressive load increase. We measured 0.3 mm for 500-N axial compression.

RoM data showed a good agreement to previously reported data of L4–5 segments (Heuer et al., 2007b). Generally, the RoM values found were slightly less than these obtained from the L4–5 segments. This discrepancy can be explained by the change in motion responses due to the different disc level tested (Plamondon et al., 1988; Schmoelz et al., 2003; Yamamoto et al., 1989). We obtained a difference between the w/oALL and w/oVA of 0.6° in flexion and 2.3° in extension for 7.5 N m. This agreed to the previously determined tendency of the L4–5 specimens with 0.4° and 4.5°, respectively. Generally, the tendencies between the defects with respect to the bending moment magnitudes were comparable to the previous findings.

This study does not reflect a clinical scenario, but it provides new data regarding surface strains and disc bulging for various defects. Due to the increase in the complexity of FE models, it is difficult to obtain data from the literature. Since the IVD is the structures, which deforms most under load, it is recommended to validate the strain distribution and the out-of-plane displacement meaning disc bulging.

Conflict of interest statement

The authors declare that neither the authors nor members of their immediate families have a current financial arrangement or affiliation with the commercial companies whose products may be mentioned in this manuscript.

Acknowledgment

This study was financially supported by the German Research Foundation (Wi-1356/10-1).

References

Acaroglu, E.R., Iatridis, J.C., Setton, L.A., Foster, R.J., Mow, V.C., Weidenbaum, M., 1995. Degeneration and aging affect the tensile behavior of human lumbar annulus fibrosus. Spine 20 (24), 2690–2701.

Brinckmann, P., 1986. Injury of the annulus fibrosus and disc protrusions. An in vitro investigation on human lumbar discs. Spine 11 (2), 149–153.

Brown, T., Hansen, R.J., Yorra, A.J., 1957. Some mechanical tests on the lumbosacral spine with particular reference to the intervertebral discs; a preliminary report. Journal of Bone and Joint Surgery (American Edition) 39-A (5), 1135–1164.

Bruehlmann, S.B., Hulme, P.A., Duncan, N.A., 2004a. In situ intercellular mechanics of the bovine outer annulus fibrosus subjected to biaxial strains. Journal of Biomechanics 37 (2), 223–231.

Bruehlmann, S.B., Matyas, J.R., Duncan, N.A., 2004b. ISSLS prize winner: collagen fibril sliding governs cell mechanics in the annulus fibrosus: an in situ confocal microscopy study of bovine discs. Spine 29 (23), 2612–2620.

Ebara, S., Iatridis, J.C., Setton, L.A., Foster, R.J., Mow, V.C., Weidenbaum, M., 1996. Tensile properties of nondegenerate human lumbar annulus fibrosus. Spine 21 (4), 452–461.

Frei, H., Oxland, T.R., Rathonyi, G.C., Nolte, L.P., 2001. The effect of nucleotomy on lumbar spine mechanics in compression and shear loading. Spine 26 (19), 2080–2089.

Goel, V.K., Monroe, B.T., Gilbertson, L.G., Brinckmann, P., 1995. Interlaminar shear stresses and laminae separation in a disc. Finite element analysis of the L3–L4 motion segment subjected to axial compressive loads. Spine 20 (6), 689–698.

Green, T.P., Adams, M.A., Dolan, P., 1993. Tensile properties of the annulus fibrosus. European Spine Journal 2, 209–214.

Heuer, F., Schmidt, H., Claes, L., Wilke, H.J., 2007a. Stepwise reduction of functional spinal structures increase vertebral translation and intradiscal pressure. Journal of Biomechanics 40 (4), 795–803.

Heuer, F., Schmidt, H., Klezl, Z., Claes, L., Wilke, H.J., 2007b. Stepwise reduction of functional spinal structures increase range of motion and change lordosis angle. Journal of Biomechanics 40 (2), 271–280.

Heuer, F., Schmitt, H., Schmidt, H., Claes, L., Wilke, H.J., 2007c. Creep associated changes in intervertebral disc bulging obtained with a laser scanning device. Clinical Biomechanics (Bristol, Avon) 22 (7), 737–744.

Heuer, F., Schmidt, H., Claes, L., Wilke, H.J., 2008a. A new laser scanning technique for imaging intervertebral disc displacement and its application to modeling nucleotomy. Clinical Biomechanics (Bristol, Avon) 23 (3), 260–269.

Heuer, F., Schmidt, H., Wilke, H.J., 2008b. The relation between intervertebral disc bulging and annular fiber associated strains for simple and complex loading. Journal of Biomechanics 41 (5), 1086–1094.

Hirsch, C., Nachemson, A., 1954. New observations on the mechanical behavior of lumbar discs. Acta Orthopaedica Scandinavica 23 (4), 254–283.

Hutton, W.C., Elmer, W.A., Boden, S.D., Hyon, S., Toribatake, Y., Tomita, K., Hair, G.A., 1999. The effect of hydrostatic pressure on intervertebral disc metabolism. Spine 24 (15), 1507–1515.

Iatridis, J.C., MaClean, J.J., Ryan, D.A., 2005. Mechanical damage to the intervertebral disc annulus fibrosus subjected to tensile loading. Journal of Biomechanics 38 (3), 557–565.

Klein, J.A., Hickey, D.S., Hukins, D.W., 1983. Radial bulging of the annulus fibrosus during compression of the intervertebral disc. Journal of Biomechanics 16 (3), 211–217.

Lotz, J.C., Colliou, O.K., Chin, J.R., Duncan, N.A., Liebenberg, E., 1998. Compression-induced degeneration of the intervertebral disc: an in vivo mouse model and finite-element study. Spine 23 (23), 2493–2506.

Meakin, J.R., Reid, J.E., Hukins, D.W., 2001. Replacing the nucleus pulposus of the intervertebral disc. Clinical Biomechanics (Bristol, Avon) 16 (7), 560–565.

Noailly, J., Wilke, H.J., Planell, J.A., Lacroix, D., 2007. How does the geometry affect the internal biomechanics of a lumbar spine bi-segment finite element model? Consequences on the validation process. Journal of Biomechanics 40 (11), 2414–2425.

Plamondon, A., Gagnon, M., Maurais, G., 1988. Application of a stereoradiographic method for the study of intervertebral motion. Spine 13 (9), 1027–1032.

Rohlmann, A., Zander, T., Schmidt, H., Wilke, H.J., Bergmann, G., 2006. Analysis of the influence of disc degeneration on the mechanical behaviour of a lumbar motion segment using the finite element method. Journal of Biomechanics 39 (13), 2484–2490.

Rohlmann, A., Burra, N.K., Zander, T., Bergmann, G., 2007. Comparison of the effects of bilateral posterior dynamic and rigid fixation devices on the loads in the lumbar spine: a finite element analysis. European Spine Journal 16 (8), 1223–1231.

Schmidt, H., Heuer, F., Simon, U., Kettler, A., Rohlmann, A., Claes, L., Wilke, H.J., 2006. Application of a new calibration method for a three-dimensional finite element model of a human lumbar annulus fibrosus. Clinical Biomechanics (Bristol, Avon) 21 (4), 337–344.

Schmidt, H., Heuer, F., Drumm, J., Klezl, Z., Claes, L., Wilke, H.J., 2007a. Application of a calibration method provides more realistic results for a finite element model of a lumbar spinal segment. Clinical Biomechanics (Bristol, Avon) 22 (4), 377–384.

Schmidt, H., Kettler, A., Heuer, F., Simon, U., Claes, L., Wilke, H.J., 2007b. Intradiscal pressure, shear strain, and fiber strain in the intervertebral disc under combined loading. Spine 32 (7), 748–755.

Schmidt, H., Heuer, F., Claes, L., Wilke, H.J., 2008. The relation between the instantaneous center of rotation and facet joint forces—a finite element analysis. Clinical Biomechanics (Bristol, Avon) 23 (3), 270–278.

Schmoelz, W., Huber, J.F., Nydegger, T., Claes, L., Wilke, H.J., 2003. Dynamic stabilization of the lumbar spine and its effects on adjacent segments: an in vitro experiment. Journal of Spinal Disorders & Techniques 16 (4), 418–423.

Shah, J.S., Hampson, W.G., Jayson, M.I., 1978. The distribution of surface strain in the cadaveric lumbar spine. Journal of Bone and Joint Surgery (British Edition) 60-B (2), 246–251.

Shirazi-Adl, S.A., Shrivastava, S.C., Ahmed, A.M., 1984. Stress analysis of the lumbar disc-body unit in compression. A three-dimensional nonlinear finite element study. Spine 9 (2), 120–134.

Stokes, I.A., 1988. Bulging of lumbar intervertebral discs: non-contacting measurements of anatomical specimens. Journal of Spinal Disorder and Techniques 1 (3), 189–193.

Sutton, M.A., McNeill, S.R., Helm, J.D., Chao, Y.J., 2000. Photomechanics advances in two-dimensional and three-dimensional computer vision. In: Rastogi, P.K. (Ed.), Photomechanics, Topics in Applied Physics, vol. 77. Springer, Berlin, Heidelberg, pp. 323–372.

Wagner, D.R., Lotz, J.C., 2004. Theoretical model and experimental results for the nonlinear elastic behavior of human annulus fibrosus. Journal of Orthopaedic Research 22 (4), 901–909.

Wenger, K.H., Schlegel, J.D., 1997. Annular bulge contours from an axial photogrammetric method. Clinical Biomechanics (Bristol, Avon) 12 (7–8), 438–444.

Wilke, H.J., Claes, L., Schmitt, H., Wolf, S., 1994. A universal spine tester for in vitro experiments with muscle force simulation. European Spine Journal 3 (2), 91–97.

Yamamoto, I., Panjabi, M.M., Crisco, T., Oxland, T., 1989. Three-dimensional movements of the whole lumbar spine and lumbosacral joint. Spine 14 (11), 1256–1260.